UNIVERSITY OF
BATH

Link to publication

University of Bath

Alternative formats
If you require this document in an alternative format, please contact:
openaccess@bath.ac.uk

MEASUREMENT AND ANALYSIS OF BUOYANCY-INDUCED HEAT TRANSFER IN AERO-ENGINE COMPRESSOR ROTORS

Richard W. Jackson **Dario Luberti** **Hui Tang** **Oliver J. Pountney**

James A. Scobie **Carl M. Sangan** **J. Michael Owen** **Gary D. Lock**

University of Bath, Bath, United Kingdom

ABSTRACT

The flow inside cavities between co-rotating compressor discs of aero-engines is driven by buoyancy, with Grashof numbers exceeding 10^{13}. This phenomenon creates a conjugate problem: the Nusselt numbers depend on the radial temperature distribution of the discs, and the disc temperatures depend on the Nusselt numbers. Furthermore, Coriolis forces in the rotating fluid generate cyclonic and anti-cyclonic circulations inside the cavity. Such flows are three-dimensional, unsteady and unstable, and it is a challenge to compute and measure the heat transfer from the discs to the axial throughflow in the compressor. In this paper, Nusselt numbers are experimentally determined from measurements of steady-state temperatures on the surfaces of both discs in a rotating cavity of the Bath Compressor-Cavity Rig. The data are collected over a range of engine-representative parameters and are the first results from a new experimental facility specifically designed to investigate buoyancy-induced flow. The radial distributions of disc temperature were collected under carefully-controlled thermal boundary conditions appropriate for analysis using a Bayesian model combined with the equations for a circular fin. The Owen-Tang buoyancy model has been used to compare predicted radial distributions of disc temperatures and Nusselt numbers with some of the experimentally determined values, taking account of radiation between the interior surfaces of the cavity.

The experiments show that the average Nusselt numbers on the disc increase as the buoyancy forces increase. At high rotational speeds the temperature rise in the core, created by compressibility effects in the air, attenuates the heat transfer and there is a critical rotational Reynolds number for which the Nusselt number is a maximum. In the cavity, there is an inner region dominated by forced convection and an outer region dominated by buoyancy-induced flow. The inner region is a mixing region, in which entrained cold throughflow encounters hot flow from the Ekman layers on the discs. Consequently, the Nusselt numbers on the downstream disc in the inner region tend to be higher than those on the upstream disc.

NOMENCLATURE

a	inner radius of disc [m]
b	outer radius of disc [m]
b'	radius of outermost thermocouple on disc diaphragm [m]
d_h	hydraulic diameter ($= 2(a-r_s)$) [m]
h_f	heat transfer coefficient based on T_f ($= q_o/(T_o\text{-}T_f)$) [W/m²K]
k	thermal conductivity of air [W/mK]
k_s	thermal conductivity of disc [W/mK]
$\dot{m}$	axial throughflow mass flow rate [kg/s]
q	heat flux [W/m²]
r	radius [m]
r_s	outer radius of shaft [m]
T	temperature [K]
v_c	core velocity relative to disc [m/s]
W	axial throughflow velocity [m/s]
β	volume expansion coefficient [K⁻¹]
ρ	density [kg/m³]
μ	dynamic viscosity [m²/s]
Ω	angular velocity [rad/s]

Dimensionless parameters

Bi	Biot number ($=h_f b/k_s$)
Bo	Buoyancy number ($=\text{Re}_\phi^2 \beta\Delta T/\text{Re}_z^2$)
Co	Coriolis parameter ($= 2\frac{|v_c|}{\Omega r}/\beta(T_{o,b}\text{-}T_{o,c})$)
Gr	Grashof number ($= \text{Re}_\phi^2 \beta\Delta T$)
Nu	Nusselt number ($=h_f r/k$)
Pr	Prandtl number
Ra	Rayleigh number ($= \text{PrGr}$)
Ro	Rossby number ($= W/\Omega a$)
Re_z	axial Reynolds number ($= \rho_f W d_h/\mu_f$)
Re_ϕ	rotational Reynolds number ($= \rho_f \Omega b^2/\mu_f$)
$\beta\Delta T$	buoyancy parameter ($= (T_{o,b} - T_f)/T_f$)
Θ	non-dimensional temperature ($= (T_o - T_f)/(T_{o,b'} - T_f)$)

1. INTRODUCTION

Predicting radial clearances, disc temperatures and stresses is a challenge for the designer of compressors striving for improved engine life, stability and aerodynamic efficiency. Figure 1 shows a simplified cross-section of a high-pressure aero-engine compressor. Cooling air flows axially through the clearance between a central shaft and the cobs at the bore of co-rotating discs. Buoyancy-induced flow and heat transfer is created when the temperature of the shroud and discs is greater than that of the air in the cavity; this affects the stresses and radial growth of the discs and, in turn, the radial clearance between the rotating tip of the compressor blades and the stationary casing in the mainstream. The buoyancy forces drive an exchange of enthalpy and momentum between the rotating cavity and the cooling flow, causing a rise in temperature in the axial throughflow. Coriolis forces create cyclonic and anti-cyclonic circulations inside the rotating cavity, a flow structure which is unsteady, unstable and three-dimensional.
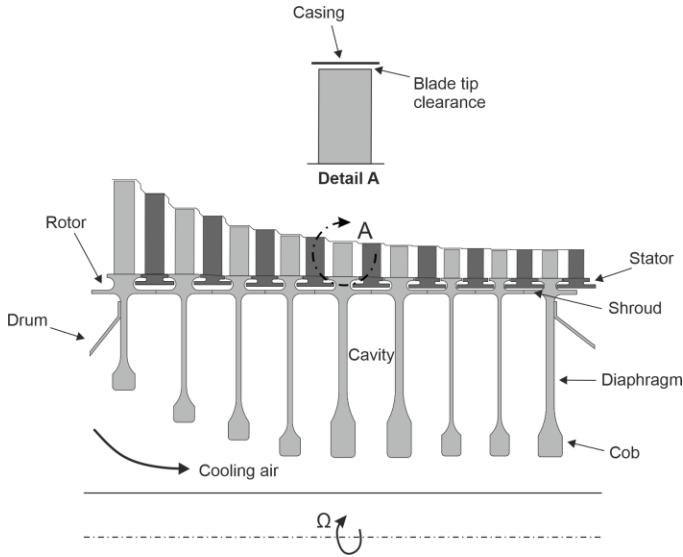

Figure 1: A simplified cross-section through a high pressure aero-engine compressor.

Figure 2 schematically illustrates the flow structure in the cavity formed by the co-rotating discs and the shroud. Here there are buoyancy-induced Ekman layers on the discs and an inviscid rotating core. The Nusselt number for the discs is given by

$$\mathrm{Nu} = \frac{h_f r}{k} \qquad (1)$$

Note that all symbols are defined in the nomenclature. At high radius, along the disc diaphragm, Nu is governed by the Grashof number, which combines the contribution of rotation and temperature difference:

$$\mathrm{Gr} = \mathrm{Re}_\phi^2 \beta \Delta T \qquad (2)$$

At engine conditions, Gr can exceed 10^{13}. The axial throughflow has a dominant influence in the inner region near the cobs; this convection zone is governed by the Rossby number (Ro), defined as the ratio of the mean axial throughflow velocity to the rotational speed of the disc:

$$\mathrm{Ro} = \frac{W}{\Omega a} \propto \frac{\mathrm{Re}_z}{\mathrm{Re}_\phi} \qquad (3)$$

The buoyancy number (Bo) is the ratio of free to forced convection in the cavity, which is proportional to the ratio of Gr to Re_z^2:

$$\mathrm{Bo} = \frac{\mathrm{Re}_\phi^2 \beta \Delta T}{\mathrm{Re}_z^2} \propto \frac{\beta \Delta T}{\mathrm{Ro}^2} \qquad (4)$$
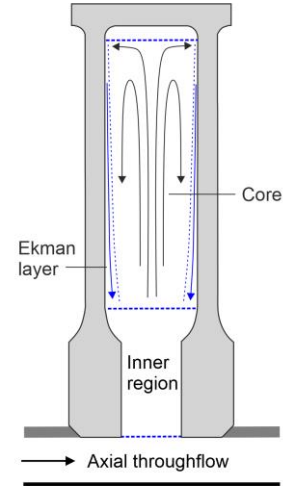

Figure 2: Compressor cavity flow structure.

This paper describes experiments conducted in a new experimental facility which models the flow and heat transfer in aero-engine compressors. The test section of the rig features four co-rotating discs enclosing three cavities. Nusselt numbers are experimentally determined from measurements of steady-state temperature in the central cavity over a range of engine-representative parameters (Gr, Ro, Re_ϕ and $\beta \Delta T$). The radial distributions of temperature were collected under carefully-controlled thermal boundary conditions appropriate for analysis using a Bayesian model combined with the equations for a circular fin. A cold axial throughflow of air was supplied between a stationary shaft and the rotating bore of the discs and the outer shroud of the cavity was heated to create the buoyancy-induced flow.

Section 2 is a brief review of the literature. Section 3 describes the three models used for the data analysis for this paper: Bayesian statistics, the circular-fin equations, and the Owen-Tang buoyancy model. Section 4 presents the Bath Compressor-Cavity Rig, the associated instrumentation and the experimental methods. Section 5 describes the experimental data analysis applied to an example experimental case ($Gr = 2x10^{12}$), including a comparison with the buoyancy model. Section 6 presents data over a range of engine-representative non-dimensional parameters. Future work is discussed briefly in Section 7 and the conclusions are described in Section 8.

2. LITERATURE REVIEW

Owen and Long [1] provide a wide-ranging review of buoyancy-induced flow in rotating cavities. The relevant dimensionless parameters for aero-engine compressors are Gr ($\sim 10^{13}$), Re_z ($\sim 10^5$), Ro ($\sim 10^0$), and $\beta\Delta T$ ($\sim 10^{-1}$). This review was extended by Luberti *et al.* [2], including discussion of the most recent and relevant experimental work from the universities at Sussex [3], Dresden [4, 5] and Beihang [6]. Luberti *et al.* [7] showed that the radial distribution of temperature has a significant effect on the disc growth and consequently on the blade clearance in a compressor. Although the growth due to the thermal stress is small relative to the total growth of the disc, it is the same magnitude as the blade clearance.

Computational fluid dynamics (CFD) cannot currently achieve accurate solutions at high Gr but large-eddy-simulation (LES) methods offer insight into the cavity flow structure and behaviour. Results from a hybrid LES/RANS simulation [3], for an open cavity with axial throughflow predict radial arms of positive and negative velocity at $Gr \sim 3x10^{12}$, indicative of the cyclonic and anticyclonic vortices expected in buoyancy-induced flow. More recent LES computations by Pitz *et al.* [8] reveal radial arms of cold fluid from the axial throughflow entering the cavity, with their radial extent increasing with Re_z; the boundary layer thickness and radial and tangential velocity profiles close to the disc surface were consistent with those predicted by a laminar Ekman layer solution.

Some engine designers use empirical formulae which are not always based on appropriate physical models. The authors have recently produced a series of publications on physically-based theoretical modelling; an overview is presented by Owen *et al.* [9].

Two important flow regimes occur in a compressor cavity and the transition between them is an important design consideration. With reference to Fig. 1, the outer shroud is hot relative to the axial throughflow for steady-state conditions (*e.g.* cruise in the flight cycle). The radial temperature gradient across the rotating cavity drives a buoyancy-induced flow at large values of Gr. Radial flow is restricted to the Ekman layers on the discs, where shear stress creates the Coriolis forces, and to non-axisymmetric vortex structures in the core, where the Coriolis forces are created by gradients of circumferential pressure inside regions of cyclonic and anti-cyclonic flow. Such phenomena, which are three-dimensional, unsteady and unstable, constitute a major challenge from the perspective of CFD.

However, the throughflow can be hotter than the shroud under transient conditions (*e.g.* accelerations or decelerations in the flight cycle). Here the flow in the cavity will be stably stratified with no buoyancy-induced convection; the heat transfer to the discs is relatively small and dominated by conduction and radiation.

Importantly, buoyancy-induced flow in rotating cavities is a conjugate problem: the temperatures of the rotating discs and the fluid core are coupled; the conduction in the discs depends on the flow structure in the fluid core between adjacent discs, and *vice versa*. As discussed below, this has a significant effect on the data analysis used in this paper.

3. REVIEW OF MODELS USED FOR DATA ANALYSIS

Three different mathematical models are used to analyse the experimental data collected using the Bath Compressor-Cavity Rig [2]. These include Bayesian statistics, the circular-fin equation, and the Owen-Tang buoyancy model. The models are described below but the reader is referred to the relevant papers for the equations used in the analysis.

3.1 Bayesian model

Thermocouple measurements are prone to several sources of error. These include conduction errors (owing to conduction down the wires), thermal-disturbance errors (caused by differences between the thermal conductivity of the thermocouples and that of the substrate), and sparseness of data (owing to insufficient thermocouples to reduce statistical uncertainties in the calculated fluxes). The instrumentation has been fitted to minimize these errors yet the resulting uncertainty in the measured temperatures was still estimated to be ±0.5 °C. Determining the heat transfer coefficient, h, from temperature measurements is an inverse problem; small uncertainties in the measurements can create very large uncertainties in the calculated values of h [10].

Bayesian statistics are widely used to solve inverse problems and Tang *et al.* [11] showed how a Bayesian model could be used to accurately determine Biot numbers, Bi, (where $Bi = h_f b/k_S$ and k_S is the thermal conductivity of the disc) from measured disc temperatures. The model assumed that there was a smooth radial distribution of Nusselt number, which was then used as the boundary condition for the *direct* solution (as opposed to the *inverse* solution) of the circular fin equation - which is discussed below - to calculate the disc temperatures. Using the Bayes theorem, the distribution of Bi was changed iteratively until satisfactory convergence was achieved between the calculated and measured temperatures.

Using simulated 'noisy' temperature measurements, Tang *et al.* [11] demonstrated the effectiveness of the Bayesian model, which produced a smooth distribution of Bi, and the computed 95% confidence interval captured the true distribution. By contrast, conventional curve-fitting of the noisy temperatures, used as boundary conditions for the inverse solution of the fin equation, resulted in large oscillations and inaccurate results. The authors also used the Bayesian model to successfully compute the Nusselt numbers, and their confidence intervals,

using disc-temperature measurements from the multi-cavity Sussex rig, which is described in [3].

3.2 Circular-fin models

The axial temperature difference across the thin diaphragm section of each disc is usually negligible [3, 12]. As the temperature distribution is axisymmetric, the circular-fin equation, which is one-dimensional, can be used to calculate the radial distribution of disc temperature. Tang *et al.* [11] used the term *special fin equation* for the diaphragm section with a constant thermal conductivity, and *general fin equation* for the case where the disc thickness and conductivity varied with radius. The *special fin equation* is used below with the Tang-Owen buoyancy model, and the *general fin equation* is used with the Bayesian model. In both cases, it is necessary to specify the temperature or heat flux at the inner and outer radii of both discs in the cavity.

The use of the fin model implicitly assumes there are no axial temperature differences within a disc. Consequently, either the convective boundary conditions on the two surfaces must be the same or one surface must be insulated; the zero axial temperature gradient is equivalent to a symmetry axis on the insulated surface. In the experiments of Atkins and Kanjirakkad [3], only one disc (which was not thermally insulated on either surface) was instrumented. To solve the fin equation, it was therefore necessary to assume that the fluxes were the same on both surfaces, which in turn meant the Nusselt numbers found from the Bayesian model were in effect the average. The flow, and therefore the Nusselt numbers, in adjacent cavities in a multi-cavity rig are generally not identical, and thus it is not possible to accurately determine the Nusselt numbers for one surface unless the other surface is insulated.

The Bath Compressor-Cavity Rig is a three-cavity rig, and the temperatures of both discs and shrouds are measured only in the central cavity; the surfaces of the outer cavities are thermally insulated to avoid the ambiguity noted above. Importantly, only one surface of a disc needs to be instrumented if the (1D) fin equation is used for the analysis, whereas both surfaces must be instrumented if a 2D solver is used. That is, for a given number of thermocouples, twice as many discs can be analysed using the fin equation.

3.3 Owen-Tang buoyancy model

A simplified representation of the assumed flow structure is shown in Fig. 2. The buoyancy model [13] assumes buoyancy-induced Ekman-layer flow on the rotating discs in the cavity and an inviscid rotating core of fluid between the Ekman layers. In practice, cyclonic and anticyclonic vortices are formed in the core, but in the model the flow is assumed to be axisymmetric.

The buoyancy model comprises the three sub-models described below: the Ekman-layer equations, compressible flow in the core, and the circular-fin equation.

The linear laminar Ekman-layer equations are solved for the discs, and the compressible adiabatic equations are solved for the core temperature; these two coupled equations are referred to here as the buoyancy equations (BEs). The circular fin equation

is used to calculate the disc temperatures, using Nusselt numbers determined from the BEs, and the calculated temperatures are then used in the BEs to update the Nusselt numbers. The coupled buoyancy and fin equations are solved iteratively until convergence is achieved. The distributions of the Nusselt numbers and disc temperature predicted by the combined fin and BEs can then be compared with the distributions obtained from the Bayesian model.

The Owen-Tang buoyancy model includes an empirical Coriolis parameter, Co, which is the ratio of buoyancy to Coriolis forces in the Ekman layers. A value Co = 0.03 was used by Tang *et al.* [12] to predict experimental data from the Sussex rig, and that value is used in this paper. (In [12], the authors assumed that, at the inner radius of the disc, the Nusselt number was zero and the core temperature was equal to that of the disc. Although these assumptions were consistent with the published experimental data, it is shown in this paper that they are not universally valid.)

Unlike the Bayesian model, the buoyancy model does not use the measured distribution of disc temperature. However, as stated above, the fin equation does require temperatures or fluxes to be specified for the boundary conditions at the inner and outer radii of the disc. (Although the 1D fin equation is used for convenience, the buoyancy equations can be readily used with 2D conduction solvers.)

The term '*experimentally-derived values*' is used in this paper to refer to the measured temperatures, and to the temperatures and Nusselt numbers determined using the Bayesian model; '*theoretical values*' refer to the temperatures and Nusselt numbers predicted from the buoyancy model.

29 tests for open cavities [12, 14] and 194 tests for closed cavities [15] have been analysed by these models over a wide range of experimental parameters, and good agreement was achieved in most cases. An important finding from the analysis of all these experiments is that - owing to the temperature rise created by the compressible flow of the core - at high rotational speeds Nusselt numbers can decrease as the speed increases. This effect has been experimentally observed in Section 6.

At *prima facie*, it might seem surprising that laminar buoyancy models are appropriate for large Grashof numbers (Gr ~ 10^{12}), where turbulent flow would be expected. However, the large Coriolis accelerations will attenuate turbulence in the fluid core and the differences between the rotational speed of the core (near solid-body rotation) and the discs is relatively small.

4. BATH COMPRESSOR-CAVITY RIG

The recently-commissioned Bath Compressor-Cavity Rig was designed and constructed in partnership with Torquemeters Ltd. Luberti *et al.* [2] present a detailed description of the facility and compare its capability with other compressor-cavity rigs at Sussex, Beihang and Dresden.

An isometric view of the rig is shown in Fig. 3 with the air inlet, disc drum, drive-shaft assembly and air outlet to the extractor shown. Bulk air is drawn through the annulus between an inner stationary shaft and an overhung rotating drum of four discs. (It was shown by Tang et al. [12] that the rotational speed of an inner shaft has no significant effect on the heat transfer

from the rotating discs.) The disc drum and a belt drive system are positioned at opposite ends of a rotating shaft, which is driven by a three-phase 30 kW motor for disc speeds up to 8,000 rpm (± 10 rpm). The throughflow was set by a variable-speed extraction unit for mass-flow rates up to 0.15 kg/s, and the flow rate was measured by a thermal mass flow meter to within +/- 5×10^{-4} kg/s.

The rig test section features four rotating titanium discs enclosing three cavities: upstream, central and downstream. Two discs in the central cavity were instrumented with thermocouples to provide the radial distribution of temperature. For the tests reported here, heat and mass exchange between the throughflow and the upstream and downstream cavities was prevented by modular, thermally-insulated inserts. The shroud of the central cavity was heated by two sets of three circular-heater elements, each element having a power rating of 2 kW; typical shroud temperatures were 100 °C.
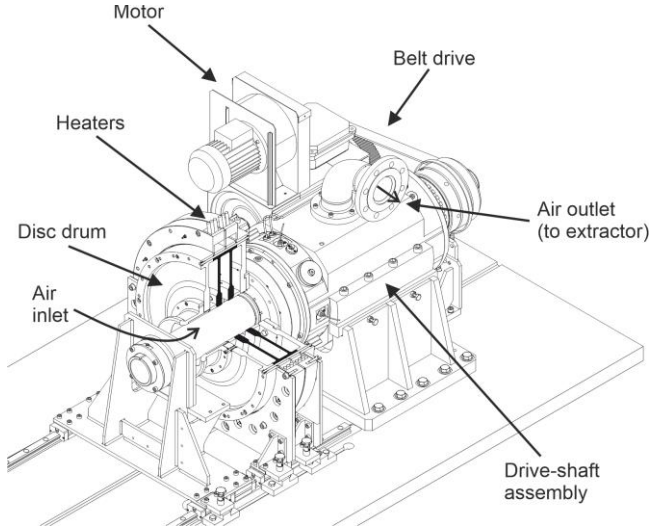

Figure 3: Overview of the experimental rig with a section view of the disc drum. The cavity test section is shaded black.

A sectional view of the central cavity showing the principal dimensions and the locations of the disc instrumentation is shown in Fig. 4. The inner surfaces of the upstream and downstream cavities (either side of the test cavity) were lined with Rohacell, a low-conductivity machinable foam (thermal conductivity 0.03 W/mK). This arrangement creates a near adiabatic boundary on the external surfaces of the discs in the test cavity; as explained in Section 2.2, this is important for the accurate application of the circular-fin model.

Both upstream and downstream discs feature a radial distribution of 28 K-type thermocouples across the cob and diaphragm regions. The thermocouple wires were potted directly into circumferential grooves machined into the titanium and filled with epoxy resin specifically selected to minimise thermal disturbance errors. The thermocouples were manufactured from a single batch of wire to minimize any variation in the Seebeck coefficient. In addition to the thermocouples on the rotating

discs, three thin foil thermocouples were secured on the underside of the disc shroud and under the cob in the bore flow using adhesive Kapton tape.

The wires of the rotating thermocouples were routed through the disc drum and drive unit to a telemetry unit at the drive end of the shaft; here the wires were pinned into the sockets of the acquisition channels in five separate transmitter modules. Each module contained a PT100 Resistance Temperature Detector (RTD) to measure the cold junction temperature. The RTDs were connected in a four-wire configuration to ensure that the wire resistance can be neglected. The uncertainty in the temperature of the cold junction, at a 1σ confidence level, is approximately ± 0.2 °C. The thermocouple and RTD data were relayed from the telemetry unit to the receiver via an antenna, and the data was then converted to a compensated temperature using a known calibration. The total estimated uncertainty of the rotating thermocouples is around ± 0.5 °C, also at a 1σ confidence level.
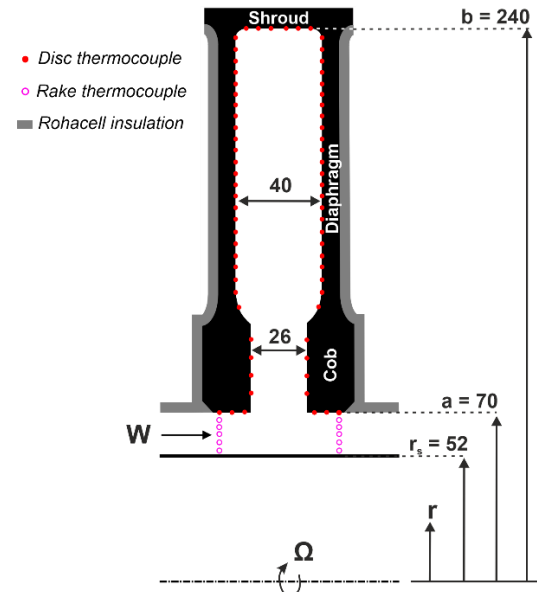

Figure 4: Cross-section of the cavity, showing thermocouple locations and the main dimensions. Dimensions in mm.

Figure 4 also shows rakes containing five K-type thermocouples, which were positioned immediately upstream and downstream of the central cavity to measure the throughflow temperature. The thermocouples in each rake were evenly spaced in the annulus between the stationary shaft and the disc bore. The mean average temperature from the upstream rake was used to calculate the inlet temperature of the throughflow, T_f, with an estimated uncertainty of ± 0.3 °C.

Steady-state temperature data was acquired at a sampling rate of 10 Hz. The normalized temperature, Θ, was used to assess whether the conditions were steady-state.

$$\Theta = \frac{T_o - T_f}{T_{o,b}{}' - T_f} \qquad (5)$$

T_f is the average temperature of the throughflow upstream of the cavity, and $T_{o,b'}$ is the temperature measured from the thermocouple at the highest radius on the diaphragm (*i.e.* closest to the shroud). A steady-state condition was defined to be when the median average of Θ for each disc thermocouple changed by less than 0.01 between a pair of ten-minute intervals. This was typically achieved after a period of 1.5 to 2 hours of continuous operation.

As part of a series of commissioning tests for the rig, a total of 30 experiments were conducted over a range of Re_ϕ, $\beta\Delta T$ and Ro. The range is shown in Fig. 5 on a series of iso-Re_ϕ lines. For each data point on the Gr versus $\beta\Delta T$ chart of Fig. 5a, two to three cases were collected at different Ro, as shown in Fig. 5b (Ro versus Re_z). The experimental range and typical uncertainty of each parameter is given in Table 1.
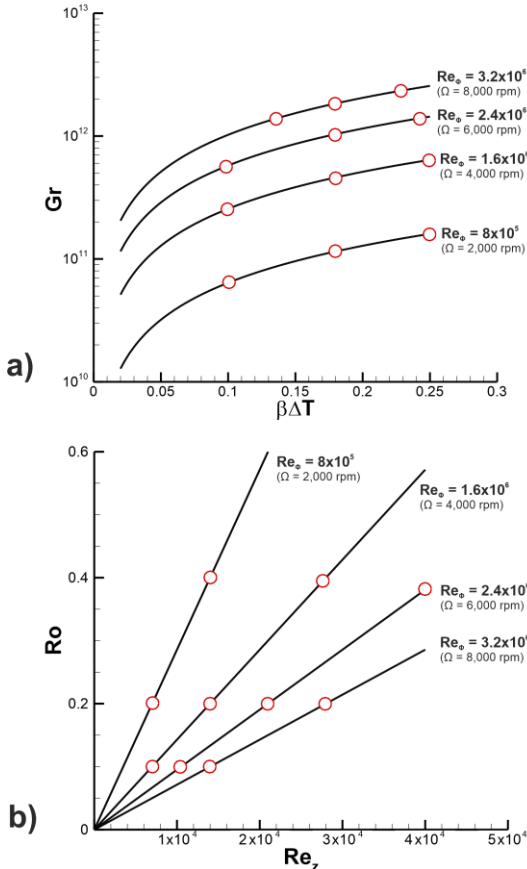
Figure 5: Test conditions, showing the variation of Gr with $\beta\Delta T$ (a) and the variation of Ro with Re_z (b).

	Parameter	Ω [rpm]	ΔT [°C]	$\dot{m}$ [kg/s]
a)	Range	2,000 – 8,000	30 - 80	0.025 – 0.139
	Uncertainty	± 10	± 1	± 5x10⁻⁴

	Parameter	$\beta\Delta T$	Re_ϕ	Gr	Re_z	Ro
	Range	0.10 - 0.25	7.7×10^5 – 3.0×10^6	7.0×10^{10} – 2.0×10^{12}	6.4×10^3 – 4.0×10^4	0.1 - 0.4
b)	Relative Uncertainty	±1.5%	±0.5%	±2%	±4%	±4%

Table 1: Dimensional (a) and non-dimensional (b) parameter ranges and typical uncertainties.

5. DATA ANALYSIS

The models used to analyse the data were described in Section 3. The section below describes the application of this analysis to a single, example experimental case ($Re_\phi = 3.0\times10^6$; $\beta\Delta T= 0.23$; Gr $= 2\times10^{12}$; Ro $= 0.2$). Section 6 presents data over the full range of engine-representative non-dimensional parameters listed in Table 1.

5.1 Conversion of temperatures to Nusselt numbers

Figure 6 shows the radial distribution of temperature across the disc, T_o, for the example case (Fig. 6a), as well as the normalized temperature, Θ (Fig. 6b). The measurement locations are indicated on the silhouette of the central cavity, which is aligned radially with the data presented. The axial throughflow is left-to-right; the closed and open symbols are for data on the upstream and downstream rotating discs, respectively. The temperatures of the axial throughflow measured upstream and downstream of the cavity are also shown.
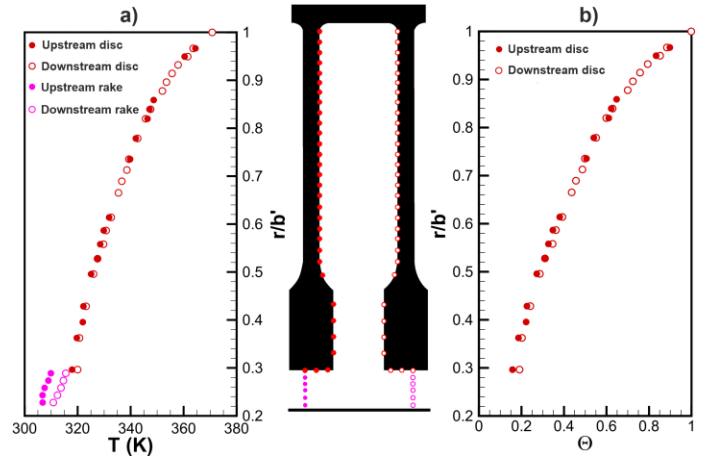
Figure 6: Raw temperatures (a) and non-dimensional temperatures (b) on the upstream and downstream disc, for an example case ($Re_\phi = 3.0\times10^6$; Gr $= 2.0\times10^{12}$; Ro $= 0.2$).

The radial temperature gradient on the rotating discs is shown clearly; this will drive buoyancy-induced flow at this large value of Gr. At radii approaching the shroud and for the greater portion of the diaphragm ($r/b' > 0.6$), the temperatures on the upstream and downstream disc mainly agree within the

6

experimental uncertainties; an average of disc temperatures is used in the analysis below. Close to the bore, especially in the region of the cobs, the downstream disc is slightly hotter than the upstream one. There is a clear rise in temperature of the axial throughflow due to an exchange in enthalpy with the rotating cavity and the heat transferred directly from the bore of the cobs.

Figure 7a shows the variation of the averaged temperature at discrete points across the radius of the disc. The Bayesian model has been applied to provide an experimentally-derived continuous radial variation shown by the line. The Bayesian model, in conjunction with the circular-fin equation, has been used to determine the variation of heat flux (from Bi) with radius; this is plotted in Fig. 7b. (Note that any two-dimensional effects in the cob region, determined using a 2D FEA solver, have been shown to be negligible.)

The heat flux, q, shown in Fig. 7b is due to both convection and radiation; the two components are separated in the discussion below. Positive q indicates that heat is transferred from the disc surface to the air in the cavity. There is a steep gradient in q for $r/b' > 0.6$, suggesting that buoyancy-induced flow dominates at high radius in the cavity. For $r/b' < 0.6$, the heat flux is relatively constant and at a significantly reduced magnitude. The data suggests two regions of heat transfer: the buoyancy-dominated region on the diaphragm, principally governed by Gr; and a forced convection zone in the region of the cobs where the mechanism for heat transfer is controlled by Re_z.
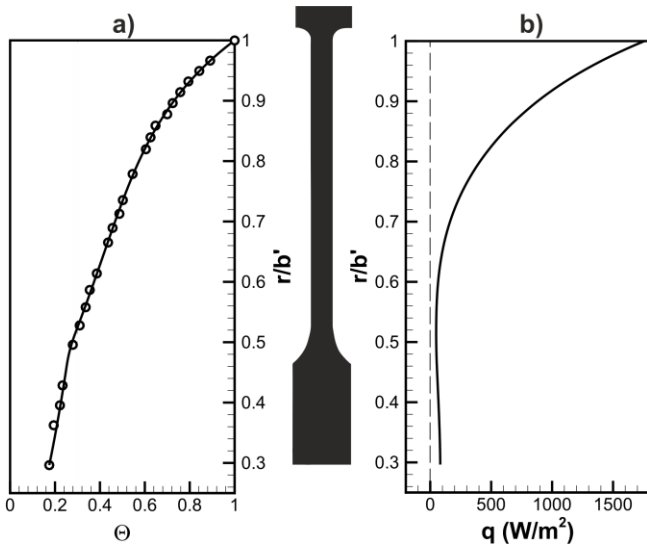

Figure 7: Radial distribution of Θ (a) and q (b), calculated from the Bayesian model.

The variation of experimentally-derived Nusselt numbers with radius is presented in Fig. 8. The shaded 95% confidence intervals of the Bayesian method in Θ (Fig. 8a) and Nu (Fig. 8b) are also shown. In a qualitatively similar manner to the distribution of q, Nu increases towards the outer radius, where the heat transfer is buoyancy-dominated.
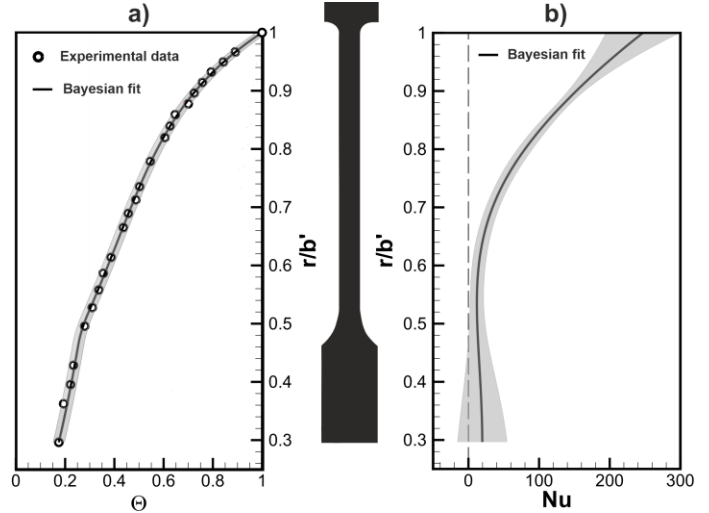

Figure 8: Radial distribution of Θ (a) and Nu (b) calculated from Bayesian model; shading shows 95% confidence intervals.

The total heat flux shown in Fig. 7b is a combination of the convective and radiative heat flux components. The shaft, shroud and the disc surfaces, which surround the cavity, were painted matt black to allow the accurate calculation of the radiant heat transfer - see Tang and Owen [16]. The two components of heat flux are presented in Fig. 9. The radiative component, marked by a red line, is subtracted from the total to give the convective contribution. The surfaces at $r/b' > 0.95$ (where the radiative heat flux is positive) lose heat due to radiation, while surfaces elsewhere gain heat. At large radius, where heat transfer is buoyancy-dominated, the radiation component is relatively small, but it is significant in the cob region.
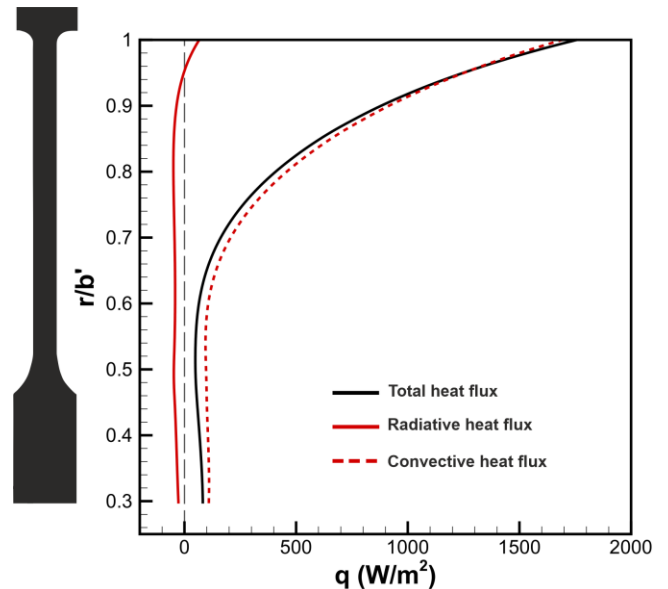

Figure 9: Effect of radiation on radial distribution of heat flux.

7

5.2 Application of Owen-Tang buoyancy model

Figure 10 compares the measured temperatures and *experimentally-derived* temperatures (left) and Nusselt numbers determined using the Bayesian model (right) with the *theoretical values* of temperature and Nusselt numbers predicted from the buoyancy model. Figure 10a shows the example experimental case ($\beta\Delta T = 0.23$, $Re_\phi = 3.0\text{x}10^6$, $Gr = 2.0\text{x}10^{12}$, Ro = 0.2, Bo = $3.0\text{x}10^3$); Fig. 10b describes a case at $\beta\Delta T = 0.14$ ($Re_\phi = 3.0\text{x}10^6$; $Gr = 1.2\text{x}10^{12}$; Ro = 0.2; Bo = $1.7\text{x}10^3$).

The Owen-Tang buoyancy model is only applied to the buoyancy-dominated region on the diaphragm, assuming a starting point of Nu = 0 at the outer radius of the cob fillet (r/b' = 0.52) before the radiation correction is applied. Compressibility effects are considered in the model, from which the radial distribution of the core temperature is calculated.
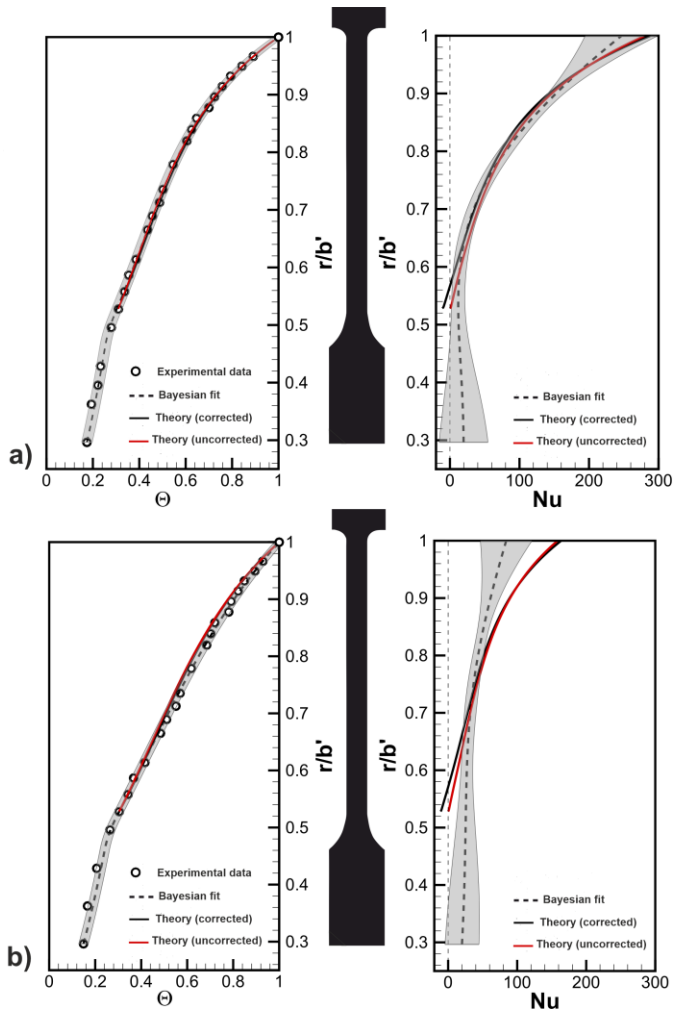

Figure 10: Effect of radiation on radial distribution of Θ and Nu calculated from Bayesian and buoyancy models; shading shows 95% confidence intervals. In (a), $\beta\Delta T = 0.23$ (Gr = $2.0\text{x}10^{12}$; Bo = $3.0\text{x}10^3$) and (b), $\beta\Delta T = 0.14$ (Gr = $1.2\text{x}10^{12}$; Bo = $1.7\text{x}10^3$). $Re_\phi = 3.0\text{x}10^6$ and Ro = 0.2 for both cases.

The buoyancy model only considers convective heat transfer and a correction for radiation must be applied in order to compare with the experimentally-derived radial variation of temperature and Nusselt number (marked 'Bayesian fit'). The red lines show the theoretical values of Θ (left) and Nu (right) from the model, and the black lines are corrected for radiation. The effect of the radiation correction on the temperatures and on Nu at large radius is small. At low radius the radiation causes a reduction in Nu to negative values.

The predicted values compare well with the experimentally-derived temperatures (left) and Nusselt numbers in the high $\beta\Delta T$, high Bo case (Fig. 10a), quantitatively agreeing within the confidence intervals. The comparison for the low $\beta\Delta T$, low Bo case (Fig. 10b) is not as good. This suggests that the effects of forced convection can be significant in the inner region between the throughflow and the core, and the buoyancy model needs to be extended to include these effects. However, the temperature distribution, which is of principal interest to the designer, is reasonably well predicted by the model even at low Bo.

6. EXPERIMENTS OVER A RANGE OF Gr, Ro, Re_ϕ

Section 5 described an example experimental case. This section presents experimentally-derived Nusselt numbers over the range of engine-representative non-dimensional parameters illustrated in Fig. 5. Rather than present the radial variation of Nu, the data is presented as an integrated radially-weighted average, $\overline{Nu}$, over the disc surface.

Figure 11 illustrates the effect of $\beta\Delta T$ and Re_ϕ on the variation of $\overline{Nu}$ with Gr; for all cases, Ro = 0.2. Consider first the physical effects of $\beta\Delta T$. For a fixed rotational speed, $\overline{Nu}$ increases with increasing $\beta\Delta T$, due to the buoyancy forces driving the convection.

As Re_ϕ increases, Gr increases but, owing to compressibility effects, the core temperature also increases; the latter tends to reduce the heat transfer. As a result, there is a critical rotational Reynolds number for which $\overline{Nu}$ is a maximum; this critical value of Re_ϕ increases as $\beta\Delta T$ increases.

Consider now the two pairs of data at common Gr (0.6 x 10^{12} and 1.2 x 10^{12}), but different Re_ϕ and $\beta\Delta T$. The juxtaposition of these points is marked in Fig. 11 by vertical dashed lines. For both pairs, $\overline{Nu}$ is significantly higher for the case with a larger $\beta\Delta T$ (increased buoyancy-induced heat transfer) and smaller Re_ϕ (reduced temperature rise in the core created by compressibility effects in the air).
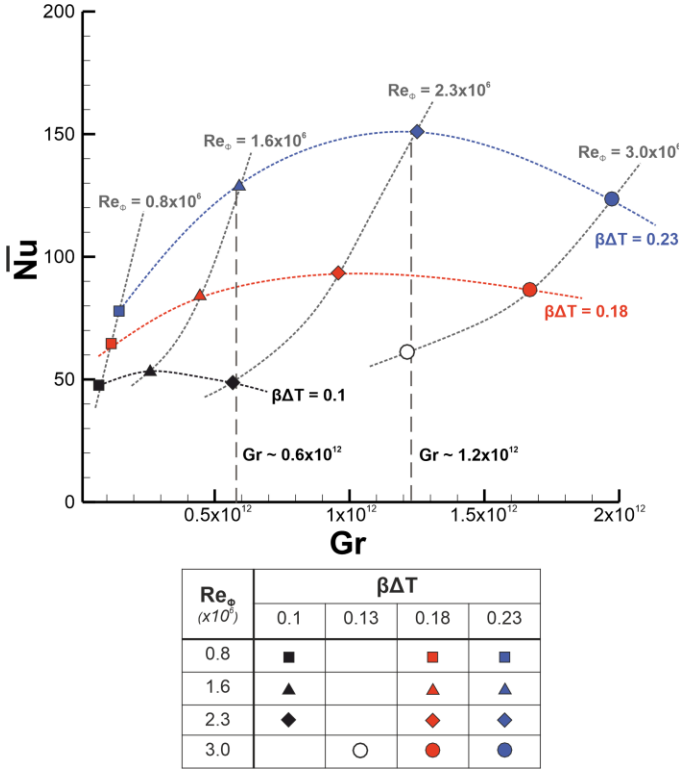
Figure 11: Effect of Re_ϕ and $\beta\Delta T$ on variation of $\overline{Nu}$ with Gr (Ro = 0.2).

it is also a mixing region in which entrained cold throughflow mixes with hot fluid from the Ekman layers. Consequently, the air temperature in the cavity tends to decrease, and the Nusselt numbers tend to increase, as Re_z increases. As Ro is proportional to the ratio Re_z/Re_ϕ, $\overline{Nu}$ therefore tends to increase as Ro increases. Conversely, for constant Ro, Bo increases as $\beta\Delta T$ increases, and - due to the stronger buoyancy forces - $\overline{Nu}$ increases as Bo increases.
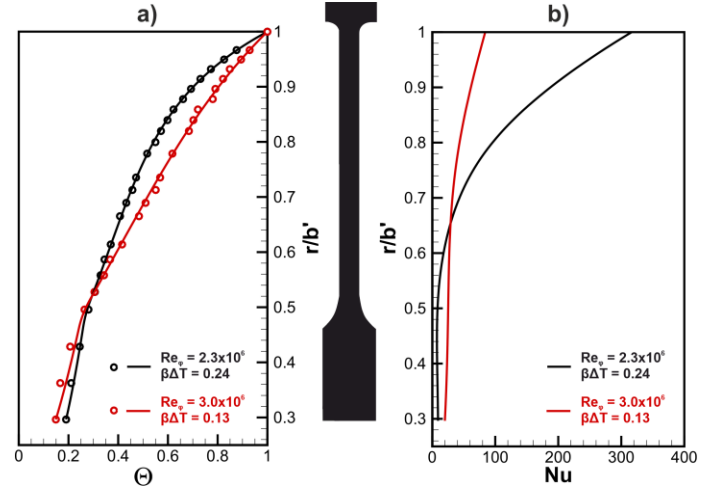

Figure 12: Effect of compressibility on radial distribution of Θ (a) and Nu (b) calculated from Bayesian model; shading shows 95% confidence intervals for Gr = 1.2×10^{12}. (Black data is taken at Bo = 3.1×10^3 and red data at Bo = 1.7×10^3).
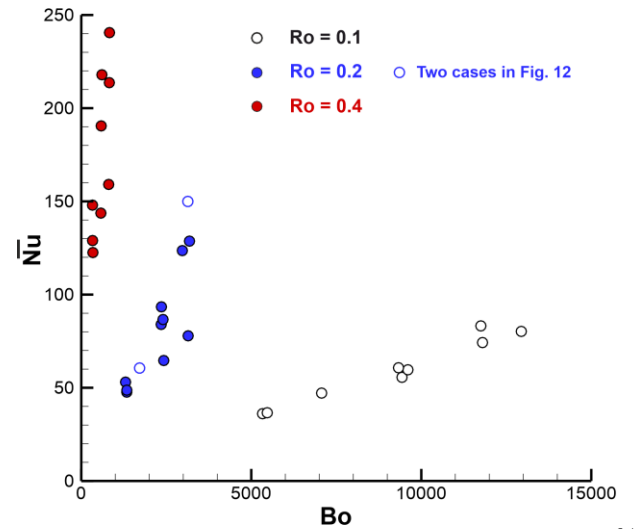
The compressibility discussed above has been reported in other papers for experiments made in different experimental rigs [12-14]. This is explored further in Fig. 12, which shows the variation of Θ (Fig. 12a) and Nu (Fig. 12b) with radius for the two conditions at Gr = 1.2×10^{12} but different Re_ϕ and $\beta\Delta T$. The Nusselt number for the case of larger $\beta\Delta T$ and lower Re_ϕ is relatively greater for $r/b' > 0.65$, where buoyancy-induced heat transfer dominates. However, for $r/b' < 0.65$ Nu $\rightarrow 0$ for the case of higher $\beta\Delta T$ (hence higher Bo at the same Ro) in the inner region; Nu for the lower $\beta\Delta T$ (hence lower Bo) case is slightly higher. This is indicative of a change in the relative dominance of the two regions of heat transfer in the cavity, *i.e.* forced convection in the inner region, and buoyancy-induced heat transfer at higher radius. The influence of the throughflow has extended further into the cavity, as reflected in the radial distribution of Θ.

The relative effects of the free and forced convection regions can be quantified by the buoyancy number, Bo, as defined by equation (4); the numerator, $Re_\phi^2 \beta\Delta T$ (equivalent to Gr) is proportional to the strength of free convection on the discs, while Re_z^2 (the denominator) is proportional to the influence of the throughflow.

Figure 13 shows the effect of Ro on the variation of $\overline{Nu}$ with Bo. It can be seen that $\overline{Nu}$ increases if either Bo or Ro increase. The effect of Ro can be explained by considering the inner region, which constitutes a combined source-sink for the cavity;

Figure 13: Effect of Ro on variation of $\overline{Nu}$ with Bo (Bo $\propto \frac{\beta\Delta T}{Ro^2}$)

The effect of the Rossby number on the radial distribution of Θ and Nu is shown in Fig. 14; here $\beta\Delta T = 0.24$, $Re_\phi = 2.3 \times 10^6$, and Gr = 1.2×10^{12}. With increasing Ro, Θ (Fig. 14a) decreases while Nu (Fig. 14b) increases across all radial locations on the disc. As stated above, the larger rate of throughflow associated

9

with increasing Ro reduces the core temperature and increases the heat transfer.
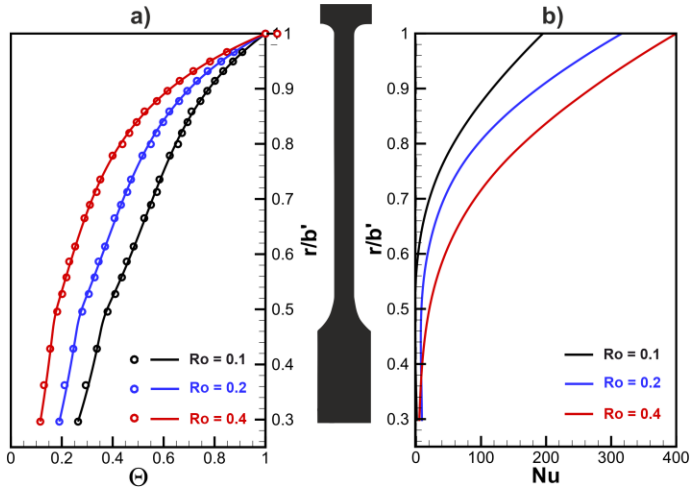

Figure 14: Effect of Ro on radial distribution of Θ (a) and Nu (b) calculated from Bayesian model ($\beta\Delta T = 0.24$; Re$_\phi$ = 2.3x10^6).

The data presented so far have been an average of the two discs in the cavity. Now the heat transfer for the upstream and downstream discs are analysed separately. Figure 15 presents the separated temperatures and Nusselt numbers, respectively, in the inner region, for a case where Ro = 0.4. The axial throughflow is left-to-right; the closed and open symbols are for data on the upstream and downstream rotating discs, respectively. Also shown are the air temperatures of the axial throughflow measured just upstream and downstream of the rotating cavity. The temperature rise of the axial throughflow is caused by heat transfer from the discs and shroud to the throughflow (Fig. 15a). The combined source-sink and mixing region, where entrained cold throughflow mixes with hot fluid from the Ekman layers, is illustrated in Fig. 15b.

There are significant differences in the cob region, where the downstream disc is hotter than the upstream one; this is consistent with toroidal vortex flow and forced convection. There is a positive value of Nu for the downstream disc and a negative value for the upstream disc. (This behavior has also been observed at high Ro in the experimental results of Gunther *et al.* [4] and the computational results of Pitz *et al.* [8].) It can be explained by the cold throughflow impinging on the downstream disc first, before recirculating, gaining enthalpy, and then transferring heat to the upstream disc.

Although it is not shown here, for $r/b' > 0.6$ (*i.e.* most of the diaphragm region where buoyancy effects dominate) the differences between the upstream and downstream values of Θ and Nu are mainly within the experimental uncertainties.
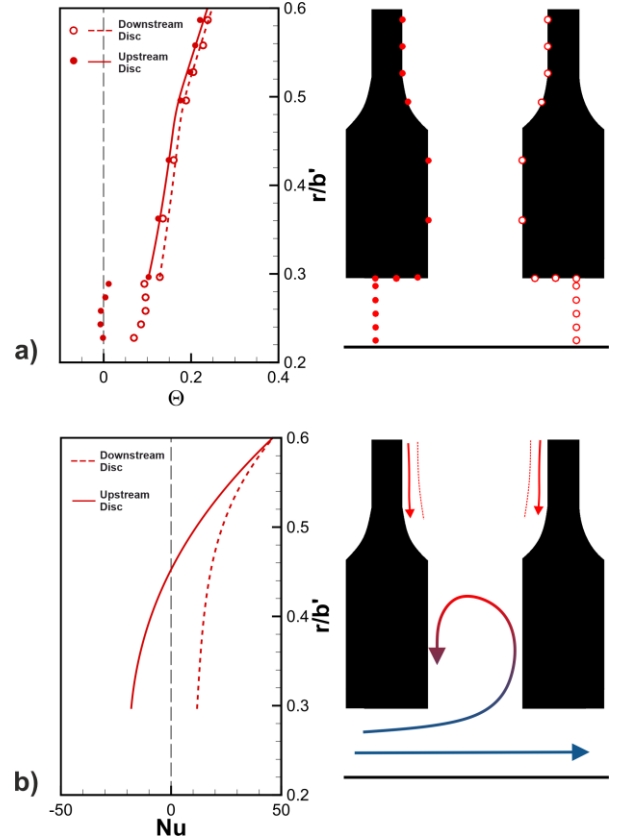

Figure 15: Radial distribution of Θ (a) and Nu (b) for the upstream and downstream discs at Ro = 0.4 ($\beta\Delta T = 0.24$; Re$_\phi$ = 2.2x10^6; Gr = 1.2x10^{12})

7. FUTURE RESEARCH

Future work will include experiments and theoretical modelling over a wider parameter range. This will involve measurements of heat transfer on the shroud and unsteady pressures on the surface of the discs; the pressure measurements will be used to determine the unsteady flow structures in the core. The temperature of the air in the cavity will be measured by a custom-made aerodynamic probe. In addition, there will be tests with different cob geometries - including the closed-cavity case with no axial clearance between the cobs - and with differential heating of the shroud to produce different temperatures for the two discs. Importantly, tests will also be conducted with heated throughflow to produce conditions in which stratified flow could occur in the cavity.

8. CONCLUSIONS

Mathematical models based on Bayesian statistics and the circular fin equation have been used to calculate Nusselt numbers using steady-state disc-temperature measurements in the Bath Compressor-Cavity Rig.

Steady-state temperature measurements were collected and analysed for a range of the important non-dimensional parameters: Re$_\phi$, $\beta\Delta T$, Gr, and Ro. The ranges of these parameters were: $0.8\text{x}10^6 < \text{Re}_\phi < 3.0\text{x}10^6$; $0.10 < \beta\Delta T < 0.25$; $7.0\text{x}10^{10} < \text{Gr} < 2.0\text{x}10^{12}$; $0.1 < \text{Ro} < 0.4$. The Nusselt numbers

were estimated using the Bayesian model applied to the inverse solution of the fin equation.

Analysis showed that, due to an increase in the buoyancy forces, the radially-weighted average disc Nusselt numbers increased with increasing $\beta\Delta T$. However, at high rotational speeds an increase in Re_ϕ could cause a decrease in Nu. This effect, which is attributed to a temperature rise in the core, is created by compressibility effects in the air.

An inner region, between the axial throughflow and the region of buoyancy-induced flow, was shown to constitute a combined source-sink for the cavity. It is also a mixing region, in which entrained cold throughflow mixes with hot fluid from the Ekman layers. Consequently, the air in the cavity tends to decrease, and the Nusselt numbers tend to increase, as Re_z increases. As the Rossby number, Ro, is proportional to the ratio of Re_z to Re_ϕ, the Nusselt numbers therefore tend to increase as Ro increases. The buoyancy number, Bo, which is the ratio of free (buoyancy-induced) and forced convection, is inversely proportional to Ro. Consequently, Nu tends to increase as Bo decreases. (No correlation has yet been found for the value of Bo at the transition from forced to free convection.)

The Owen-Tang buoyancy model has been used to compare predicted radial distributions of disc temperatures and Nusselt numbers with the experimentally determined distributions, taking account of radiation between the inner surfaces of the cavity. Although there was good agreement with the temperature measurements at the higher values of Bo (that is, at the smaller values of Ro and the larger values of $\beta\Delta T$), the agreement was less good at the smaller values of Bo. This suggests that the effects of forced convection can be significant in the inner region, and the buoyancy model may need to be extended to include these effects.

REFERENCES
[1] Owen, J. M., and Long, C. A., 2015, "Review of Buoyancy-Induced Flow in Rotating Cavities," *ASME. J. Turbomach.,* **137**(11), p. 111001.
[2] Luberti, D., Patinios, M., Jackson, R., Tang, H., Pountney, O., Scobie, J., Sangan, C., Owen, J. M., Lock, G. D., 2019, "Design and Testing of a Rig to Investigate Buoyancy-Induced Heat Transfer in Aero-Engine Compressor Rotors," ASME Paper No. GT2020-14422. [Submitted]
[3] Atkins, N. R., Kanjirakkad, V., 2014, "Flow in a rotating cavity with axial throughflow at engine representative conditions", ASME paper GT2014-271747.
[4] Günther, A., Uffrecht, W., Odenbach, S., 2012, "Local measurements of disc heat transfer in heated rotating cavities for several flow regimes", *ASME. J. Turbomach.*, Vol. 134, 051016.
[5] Diemel, E., Odenbach, S., Uffrecht, W., Rey Villazon, J., Guijarro Valencia, A., Reinecke, M., 2019, "High speed single cavity rig with axial throughflow of cooling air: rig structure and periphery", ASME paper GT2019-91265.
[6] Quan, Y., Han, D., Xu, G., Wen, J., Luo, X., 2018, "Convective heat transfer of a rotating multi-stage cavity with axial throughflow", *Int. J. Heat Mass Transfer*, Vol. 119, 117-127.
[7] Luberti, D., Tang, H., Scobie, J., Pountney, O., Owen, J. M., Lock, G. D., 2019, "Influence of Temperature Distribution on Radial Growth of Compressor Discs", ASME paper GT2019-91848.
[8] Pitz, D. B., Chew, J. W. and Marxen, O., 2019, "Effect of an Axial Throughflow on Buoyancy-Induced Flow in a Rotating Cavity, *Int. J. Heat Fluid Flow*, Vol. 80, 108468.
[9] Owen, J. M., Tang, H., and Lock, G. D., 2018, "Buoyancy-Induced Heat Transfer inside Compressor Rotors: Overview of Theoretical Models," *Aerospace*, **5**(1), pp. 1-22.
[10] Owen, J. M., 1979, "On the Computation of Heat-Transfer Coefficients from Imperfect Temperature Measurements", *J. Mech. Eng. Sci.*, **21**(5), 323-334.
[11] Tang, H., Shardlow, T., and Owen, J. M., 2015, "Use of Fin Equation to Calculate Nusselt Numbers for Rotating Discs," *ASME. J. Turbomach.*, **137**(12), p. 121003.
[12] Tang, H., Puttock-Brown, M. R., and Owen, J. M., 2018, "Buoyancy-Induced Flow and Heat Transfer in Compressor Rotors", *ASME J. Eng. Gas Turb. Power*, **140**(7).
[13] Owen, J. M., and Tang, H., 2015, "Theoretical Model of Buoyancy-Induced Flow in Rotating Cavities," *ASME. J. Turbomach.,* **137**(11), p. 111005.
[14] Tang, H., and Owen, J. M., 2017, "Effect of Buoyancy-Induced Rotating Flow on Temperatures of Compressor Disks", *ASME J. Eng. Gas Turb. Power,* **139**(6), pp. 1-10.
[15] Tang, H., and Owen, J. M., 2018, "Theoretical Model of Buoyancy-Induced Heat Transfer in Closed Compressor Rotors", *ASME J. Eng. Gas Turb. Power*, **140**(3).
[16] Tang, H., and Owen, J. M., 2019, "Effect of Radiation Inside Compressor Rotors", *ASME J. Heat Transfer.* [Submitted]